The Astrophysical Journal, 590:533–546, 2003 June 10

CONSTRAINTS ON CORONAL MASS EJECTION DYNAMICS FROM SIMULTANEOUS RADIO AND WHITE-LIGHT OBSERVATIONS

M. J. Reiner
Center for Solar Physics and Space Weather, Catholic University of America, Washington, DC 20064; and NASA Goddard Space Flight Center, Greenbelt, MD 20771

A. Vourlidas
Center for Earth Observing and Space Research, Institute for Computational Sciences, George Mason University, Fairfax, VA 22030

O. C. St. Cyr
NASA Goddard Space Flight Center, Code 682, Greenbelt, MD 20771

J. T. Burkepile
High Altitude Observatory, National Center for Atmospheric Research, Boulder, CO 80307

R. A. Howard
E. O. Hulburt Center for Space Research, Naval Research Laboratory, 4555 Overlook Avenue, SW, Washington, DC 20375

M. L. Kaiser
Laboratory for Extraterrestrial Physics, NASA Goddard Space Flight Center, Greenbelt, MD 20771; aastex-help@aas.org

N. P. Prestage
IPS Radio and Space Services, Culgoora Solar Observatory, Narrabri, NSW 2390, Australia

and

J.-L. Bougeret
Departement de Recherche Spatiale, Observatoire de Paris, 5 Place Jules Janssen, F-92195 Meudon Cedex, France
Received 2002 April 8; accepted 2003 February 5

ABSTRACT

Simultaneous radio and white-light observations are used to deduce information on the dynamics of two coronal mass ejection (CME) events that occurred about 2 hr apart on 2001 January 20 and that were associated with eruptions from the same active region on the Sun. The analysis combines both space-based and ground-based data. The radio data were obtained from the WAVES experiment on the *Wind* spacecraft and from the Culgoora radiospectrograph in Australia. The white-light data were from the LASCO experiment on *SOHO* and from the Mk4 coronameter at the Mauna Loa Solar Observatory. For these CME events we demonstrate that the frequency drift rate of the type II radio emissions, generated by the shocks driven by the white-light CMEs, are consistent with the plane-of-sky height-time measurements, provided that the propagation direction of the CMEs and their associated radio sources was along a radial line from the Sun at a solar longitude of $\sim$E50°. These results imply that the "true" CME speeds were estimated to be $\sim$1.4 times higher than the measured plane-of-sky speeds and that the CMEs originated from solar eruptions centered near E50°. This CME origin is consistent with the known active region and flare site associated with these two CME events. Furthermore, we argue that the type II radio emissions generated by these CMEs must have originated in enhanced density regions of the corona. We investigate whether the type II radiation could have originated in one or more dense coronal streamers, whose densities were estimated from the polarization brightness measurements made by LASCO at that time. Finally, we use these radio and white-light observations to speculate about the dynamics and scales involved in the interaction between these two CMEs.

Subject headings: solar-terrestrial relations — Sun: activity — Sun: corona — Sun: flares — Sun: radio radiation

1. INTRODUCTION

A notable limitation of white-light coronagraph observations for determining the dynamics of coronal mass ejections (CMEs) is that they record only the image of a CME projected onto the plane of the sky. Although this limitation is not a serious drawback for CMEs that occur on or near the solar limb, it becomes more serious as the solar longitude of the CME origin nears central meridian. For these latter CMEs, both the plane-of-sky speed and acceleration, derived from the white-light coronagraph images, can differ significantly from the "true" or radial CME speed and acceleration (by factors of 2 or 3; Howard et al. 1982). Although several attempts have been made to correct for the plane-of-sky projections by using simple CME models or simple geometries (Fisher & Munro 1984; Eselevich & Filippov 1991; Hundhausen, Burkepile, & Cyr 1994; Plunkett et al. 1998; Leblanc et al. 2001), the fact remains that the actual three-dimensional structure of white-light CMEs remains largely unknown. Furthermore, the three-

dimensional structure of a CME may differ significantly from one CME event to another so that no CME model is expected to be universally applicable. It is therefore not a priori clear how to make corrections to the plane-of-sky coronagraph measurements for a given CME event—even when the solar longitude of the CME origin is known.

On the other hand, shocks driven by the CMEs observed in the white-light coronagraph often generate (type II) radio emissions in the decametric to hectometric wavelength regime (Kaiser et al. 1998; Reiner et al. 2000a; Gopalswamy et al. 2000). These radio emissions are generated via the plasma emission mechanism from electrons accelerated by the CME-driven shocks (Bale et al. 1999) and are observed at the fundamental and/or harmonic of the plasma frequency. Since the plasma frequency in kilohertz is $f_p = 9\sqrt{n_p}$, the radio observations directly measure the plasma density n_p cm^{-3} in the radio source region.

At the decametric to hectometric wavelengths we do not yet have the capability of constructing images of the type II radio sources that could then be directly compared with the white-light coronagraph images (Jones et al. 2000). However, the Low Frequency Array (LOFAR), which will become operational in 2006, will provide radio imaging at decametric to metric wavelengths (~10–240 MHz).[1] Currently, the decametric to kilometric radio emission intensities are measured by fixed-frequency receivers on several spacecraft. Such fixed-frequency radio intensity measurements are made at a large number of radio frequencies and are then plotted together in order of decreasing frequency to form a radio dynamic spectrum. This dynamic spectrum is a plot of the intensity of the radio emissions as a function of frequency (vertical axis) and time (horizontal axis). It makes sense to plot the radio data in this format because high frequencies correspond to the propagation of the CME in the corona where the plasma density is high, whereas progressively lower radio frequencies are produced as the CME/shock propagates through the high corona and into the interplanetary medium, where the plasma density continually decreases. Thus as the CME propagates through the corona the type II radio emissions observed in the radio dynamic spectrum will drift to continually lower frequencies. The measured rate of the frequency drift of these type II radio emissions is related to the speed of the shock driven by the CME. Unlike the case for the white-light observations, the frequency drift rate of the type II radio emissions measures the radial (unprojected) speed and acceleration of the propagating disturbance causing it. We therefore assume that the dynamics of the shock, as deduced from the frequency-drifting radio emissions, can serve as a proxy for the dynamics of the driver CME.

To deduce the value of the " true " speed or " true " acceleration of the CME/shock from these frequency-drifting radio observations, however, the relationship between the electron density and the height above the corona has to be known; i.e., one has to have (or assume) a coronal density model. In general, the coronal density profile that applies to the radio-emitting region(s) for a given CME event is not precisely known. In practice, what is normally done is to assume some universal coronal electron density model, obtained either from white-light observations (Newkirk 1967; Saito 1970) or from radio observations (Fainberg & Stone 1971; Leblanc, Dulk, & Bougeret 1998). Thus in the interpretive context of such an assumed coronal density model, one can derive from the radio data the " true " speed (and acceleration) of the CME/shock. But the CME dynamics derived in this way is correct only to the extent that the coronal density profile correctly represents the densities in the radio-emitting region(s). On the other hand, for a given CME event the coronal density model can to some extent be checked since the coronal electron density as a function of height can be derived from the white-light coronagraph polarized brightness measurements.

It is clear from the above discussion that both the white-light and radio observations have limitations that severely hinder the determination of the true CME dynamics from these data. On the other hand, since the radio and white-light observations are related to different physical quantities (true height vs. plane-of-sky height), the above discussion suggests that by combining both the white-light and radio observations for a given CME event and by requiring that the dynamics implied by these simultaneous observations be mutually consistent, i.e., that the height-time information deduced from the white-light CME be consistent with the frequency drift rate observed for the radio emissions, one may be able to overcome the limitations inherent in each of these measurements (plane-of-sky projection for white-light, and density model for radio) and thereby deduce a closer approximation to the true CME dynamics. Furthermore, the simultaneous comparison of radio and white-light observations may provide additional insights into both the nature of the CME dynamics in the corona and interplanetary medium and the nature of the source region(s) generating the radio emissions.

In this paper we illustrate how such an analysis might be implemented to estimate the true dynamics of a CME by requiring consistency between the radio and white-light observations for two CME events that occurred on 2001 January 20. Because these two CMEs, occurring about 2 hr apart, originated from eruptions in the same active region, these events provided a unique opportunity to compare the dynamics of the two CMEs deduced from the simultaneous radio and white-light observations, to determine any significant changes in the coronal densities between the two events, and to study the interaction of these CMEs. Specifically, assuming that the shock was close to the leading edge of the CME and that its standoff distance was constant, and assuming the Saito coronal density model, appropriately modified for the condition in the corona at the time of these events, we will show that the dynamics implied by the frequency drift rate of the type II radio emissions and by the white-light height-time data is consistent with a CME launch angle and propagation direction from ~E50°, which, in turn, is consistent with the known flare site and active region associated with these two CME events. We will further show that the required consistency between the radio and white-light observations implies that the radio emissions for both CME events must have been generated in enhanced density regions, such as a coronal streamer. Then, using coronal densities deduced from the LASCO polarized brightness measurements, we will try to determine whether the coronal streamers observed at that time may have had sufficient density to account for the observed radio emissions. Finally, we will use the radio and white-light observations to measure some characteristics of the interaction between the two CMEs.

[1] See http://www.lofar.org/.

2. DESCRIPTION OF INSTRUMENTS USED IN THIS INVESTIGATION

The radio instruments used in this investigation were the WAVES experiment on the *Wind* spacecraft (Bougeret et al. 1995) and the ground-based radiospectrograph at Culgoora (Prestage et al. 1994). The white-light observations were made with the LASCO coronagraph on the *SOHO* spacecraft (Brueckner et al. 1995) and with the Mark-IV (Mk4) white-light K coronameter at the Mauna Loa Solar Observatory (MLSO; Elmore et al. 2003).

The WAVES instrument on the *Wind* spacecraft includes several radio receivers that cover the frequency range from 4.0876 kHz to 13.825 MHz (Bougeret et al. 1995). The instruments used in the present analysis were two superheterodyne (step-tuned) receivers. The high-frequency (RAD2) receivers sweep 256 frequency channels from 1.075 to 13.825 MHz in 16.192 s, with a frequency resolution of 50 kHz and a bandwidth of 20 kHz. The low-frequency (RAD1) receivers cover the frequency range from 20 to 1040 kHz at 32 discrete frequencies (selected from 256 frequency channels), with a highest sampling rate of 45.8 s and a bandwidth of 3 kHz. The RAD2 receivers are connected to a dipole antenna (7.5 m elements) in the spacecraft spin plane and a dipole antenna (with 5.28 m elements) along the spacecraft spin axis. The RAD1 receivers are connected to a dipole antenna (50 m elements) in the spacecraft spin plane and the dipole antenna along the spacecraft spin axis. The spin axis of the *Wind* spacecraft (spin rate = 3 s) is approximately perpendicular to the ecliptic plane. The *Wind* spacecraft, which was launched in 1994 November, executes complex orbits that include excursions to the Lagrange point (L1) and a series of near-Earth passes. At the time of the observations presented here the *Wind* spacecraft was far from Earth, at (−4.00, +231.91, −16.32) GSE, during one of its distant prograde orbits.

The ground-based Culgoora radio spectrograph near Narrabri, Australia, has been continuously monitoring solar radio emissions since 1992 (Prestage et al. 1994). It operates in the frequency band from 18 MHz to 1.8 GHz with a sampling rate of 3 s. It observes the Sun from 2000 to 0800 UT daily.

The LASCO coronagraph on the *SOHO* spacecraft has three optical systems with overlapping and concentric fields of view (Brueckner et al. 1995). The *SOHO* spacecraft is located at L1, from where it can continuously monitor the Sun. The analyses in this paper use images recorded on 2001 January 20 with the C2 (2–7 $R_\odot$) and C3 (3.7–32 $R_\odot$) coronagraphs. The nominal C2 image cadence is 24 minutes. These coronagraphs are equipped with broadband color filters and a set of polarizers to determine the degree of polarization of the coronal brightness. The electron density profile in the corona can be estimated by inverting either polarized brightness measurements (van de Hulst 1950) or total brightness measurements once the contribution of the F corona has been modeled and removed (Hayes, Vourlidas, & Howard 2001).

The Mk4 white-light K coronameter at MLSO (Elmore et al. 2003) has a field of view from 1.08 to 2.85 $R_\odot$, with a 3 minute cadence and an angular resolution of about 20″. It observes the K corona in visible light over the wavelength range from 700 to 950 nm. The Mk4 K coronameter, which became operational in 1998 October, is able to detect events farther away from the plane of the sky because of the improved signal-to-noise ratio and operates daily from about 1700 to 2200 UT.

3. ANALYSIS OF 2001 JANUARY 20 CME/RADIO EVENTS

On 2001 January 20 NOAA reported two M-class X-ray flares (corresponding to fluxes less than 10^{-5} W m^{-2}). The first M1.2 flare was observed between 1833 and 1859 UT, with peak at 1847 UT. This X-ray event was associated with a 2F optical flare from NOAA active region 9313 at S07°E40°, observed from ~1840 to 2002 UT, with maximum around 1853 UT. The EIT instrument on *SOHO* observed the flare in its 1848 UT image (image cadence at that time was about 12 minutes), followed by a clear coronal dimming to the south of the flare site beginning at 1913 UT, which is a typical signature of the liftoff of a CME (Thompson et al. 1998). The first visual sighting of the associated white-light CME (hereafter CME1) by MLSO was at 18:50:25 UT at ~1.61 $R_\odot$ and was tracked out to ~2.17 $R_\odot$ at 19:02:15 UT. The LASCO coronagraph first observed the CME at ~4.7 $R_\odot$ at 19:31:50 UT in the C2 coronagraph. Figure 1*a* shows a composite of the Mk4 and LASCO images of CME1 at 18:54:14 and 19:31:50 UT, respectively.

About 2 hr later, *GOES-8* recorded a M7.7 X-ray flare between 2106 and 2132 UT, with peak at 2120 UT. This event was associated with a 2B optical flare from S07°E46°, observed from 2108 to 2226 UT, with maximum at 2119 UT. The flare associated with this second event was also observed by the EIT instrument on *SOHO* beginning at 2112 UT. A second CME (hereafter CME2) was observed by MLSO from 1.33 $R_\odot$ at 21:13:58 UT to 2.13 $R_\odot$ at 21:19:54 UT. The LASCO instrument observed this CME starting at 21:30:08 UT at about 3.81 $R_\odot$. Figure 1*b* shows a composite of the Mk4 and LASCO images of CME2 at 21:16:23 and 21:30:08 UT, respectively. Finally, Figure 1*c* shows the C3 coronagraph image of both CME1 and CME2 at 21:42:05, UT when CME1 was at 12.91 $R_\odot$ and CME2 was at 5.43 $R_\odot$. Figure 1*d* shows the CMEs at 23:42:31 UT after they merged at a plane-of-sky distance of ~20 $R_\odot$.

3.1. *Radio Signatures of the 2001 January 20 CME Events*

The dynamic spectrum in Figure 2*a* shows the intensity (red being most intense) of the radio data from 1800 to 2400 UT on 2001 January 20 in the frequency range between 316 kHz and 13.825 MHz measured by the RAD1 and RAD2 radio receivers of the WAVES experiment on the *Wind* spacecraft. Two very intense complex type III–like radio emissions were observed beginning at ~1847 and ~2115 UT, respectively. It has been previously demonstrated (Reiner & Kaiser 1999a; Reiner, Kaiser, & Bougeret 2001) that such complex type III–like radio emissions are the first radio signatures indicating the liftoff of a CME on the Sun, although they are not actually produced by the CME. They are probably produced by the changing magnetic field configuration in the low corona, which allows energetic electrons, produced by the associated solar flare, to escape into the interplanetary medium (Reiner et al. 2000b). The propagating CMEs, on the other hand, produced the slowly frequency-drifting sporadic type II radio emissions that are most visible in the expanded dynamic spectra shown in Figures 2*b* and 2*c* (see below).

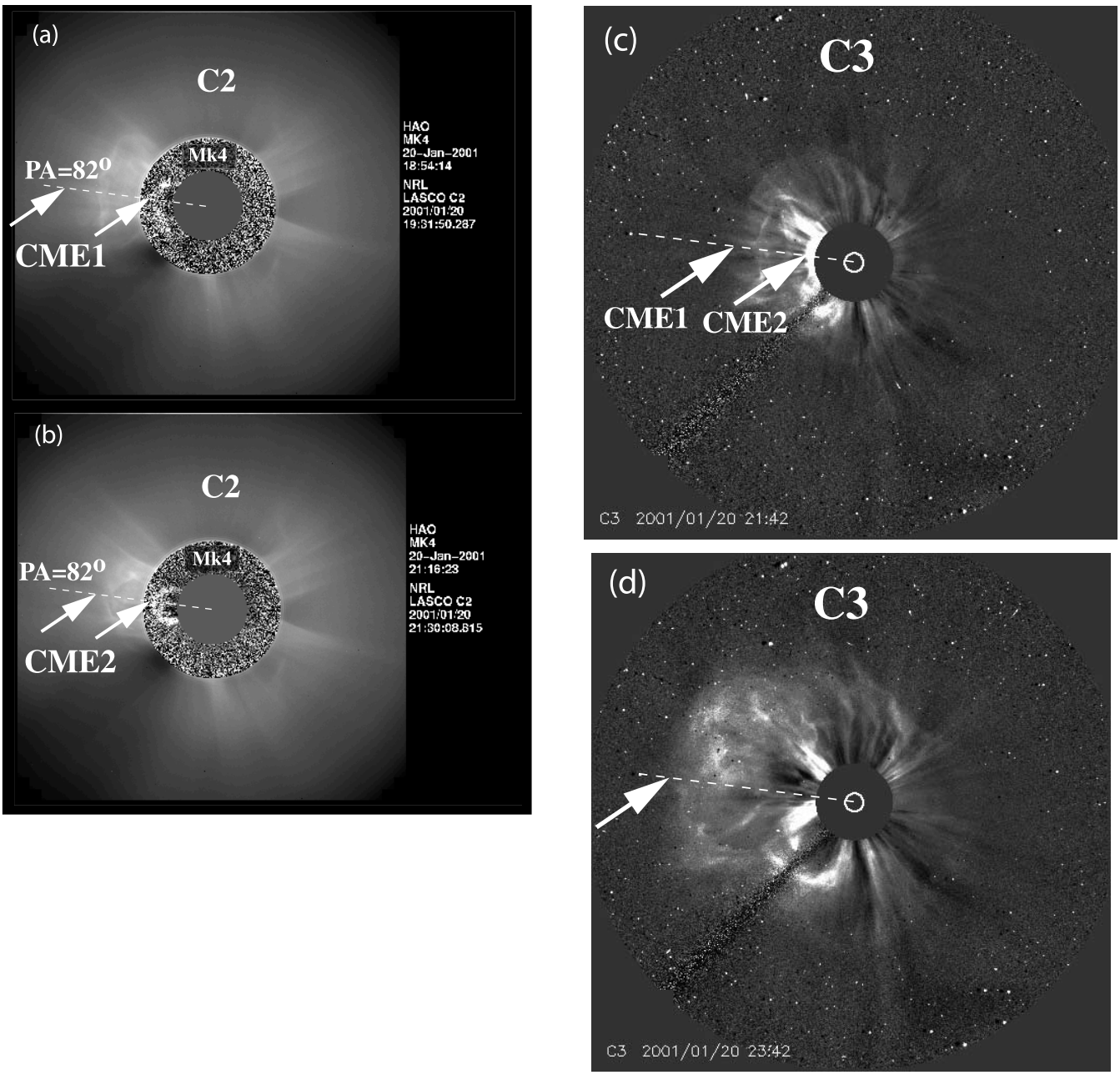

FIG. 1.—White-light MLSO/Mk4 and *SOHO* LASCO images of the two CME events observed on 2001 January 20. (*a*) Mk4 and C2 coronagraph images at 18:54:14 and 19:31:50 UT, respectively, showing CME1; (*b*) Mk4 and C2 coronagraph images at 21:26:23 and 21:30:08 UT, respectively, showing CME2; (*c*) C3 coronagraph at 21:42:05 UT, showing both CME1 and CME2; and (*d*) C3 coronagraph at 23:42:31 UT, showing the merging of CME1 and CME2.

Because of its relatively slow speed, CME1, which was ejected from the Sun at ~1840 UT (see below), produced only a short episode of decametric type II radio emissions between 1913 and 1916 UT (when CME1 was at ~3 $R_{\odot}$), drifting from ~7.2 to 6.5 MHz at the fundamental and from greater than 13.8 to 13 MHz at the harmonic of the plasma frequency (Fig. 2*b*). CME2, which lifted off at ~2110.2 UT (see below) and which was traveling twice as fast as CME1, produced complex frequency-drifting type II emissions that drifted from ~14 MHz to ~450 kHz between ~2122 and 2320 UT (Fig. 2*c*), corresponding to the propagation of the CME from the high corona (~2.5 $R_{\odot}$) into the interplanetary medium.

As we will see, these type II radio emissions continued to drift to lower frequency as CME2 propagated from the corona into the interplanetary medium, even after the two CMEs interacted, i.e., after ~2311 UT (see below). At about 2248 UT, the frequency bandwidth and intensity of the low-frequency type II radiation increased rather suddenly (see Fig. 2*a*), suggesting that this may have been the time of first contact between the two CMEs, i.e., the time that the leading edge of CME2 encountered the plasma ejecta material behind the leading edge of CME1 (Gopalswamy et al. 2001; see discussion).

For CME2, a metric-wavelength type II radio burst was also observed by the ground-based Culgoora radiospectrograph (see Fig. 2*c* and below). Both fundamental and harmonic emissions were simultaneously observed. The fundamental emission drifted semicontinuously from 160 to 18 MHz between 2112 and 2120 UT, and the harmonic drifted

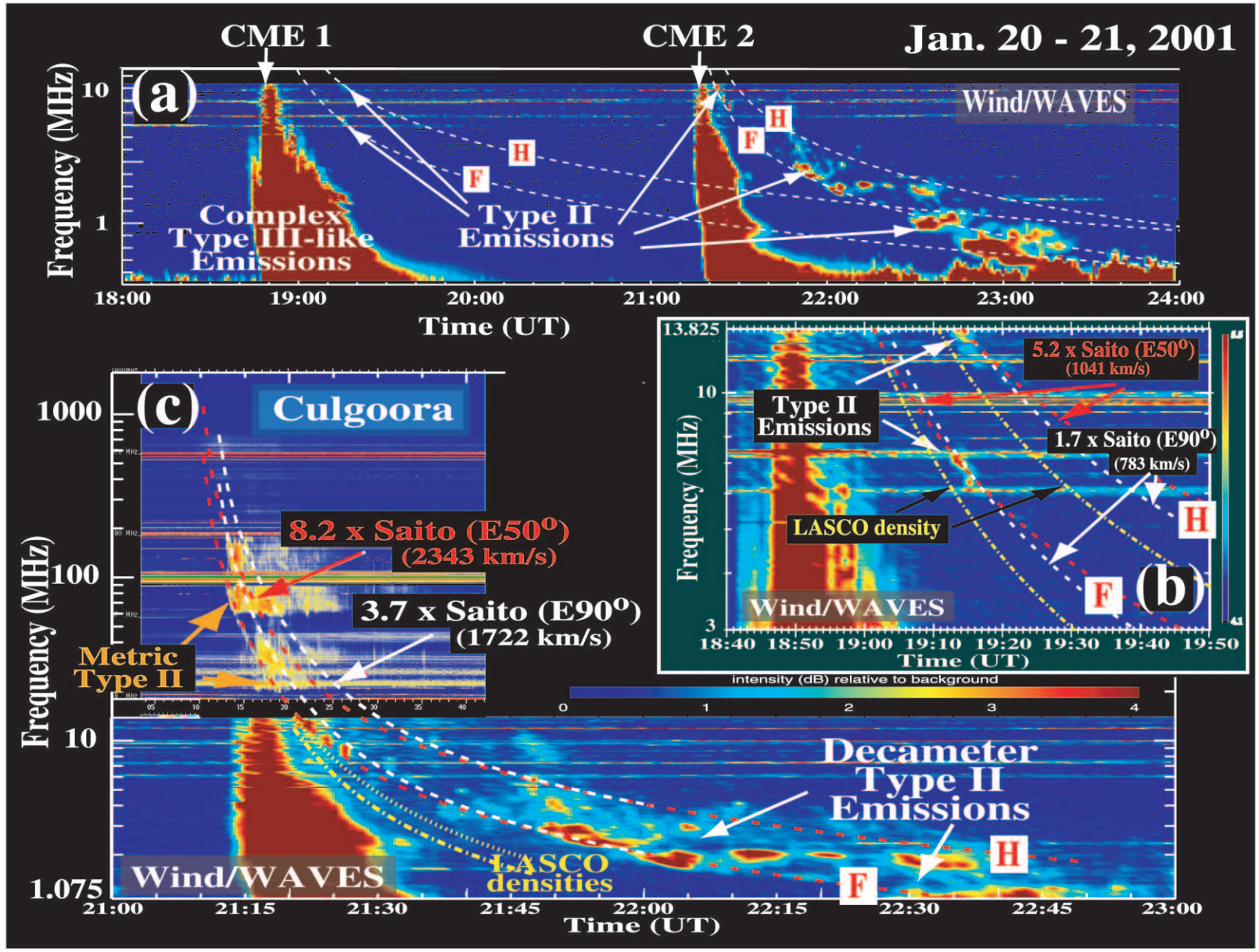

FIG. 2.—(*a*) Dynamic spectrum from the *Wind* WAVES experiment in the frequency range between 316 kHz and 13.825 MHz from 1800 to 2400 UT on 2001 January 20, showing the decametric to kilometric type II radio emissions associated with CME1 and CME2. (*b*) Dynamic spectrum, showing details of the radio emissions associated with CME1. The various curves on this plot are explained in the text. (*c*) Dynamic spectra from Culgoora and from *Wind* WAVES, showing details of the metric to hectometric radio emissions associated with CME2. The curves on this plot are also explained in the text.

from 250 to 20 MHz between 2113 and 2122 UT. The shock speed estimated from the frequency drift rate was ~1600 km s^{-1}. Although in general it is probably not the case that all metric type II radio bursts are produced by CME shocks (Gopalswamy et al. 1998; Reiner & Kaiser 1999b; Reiner et al. 2000a; Cliver, Webb, & Howard 1999), we will argue below, on the basis of the consistency between the radio and white-light data, that this metric type II burst was likely generated by CME2.

On the metric radiospectrograph there are also additional emissions at later times, some of which could also be interpreted as type II emissions. Although these additional emissions are rather ambiguous, there could be a second type II burst drifting from about 180 to 55 MHz from 2117 to 2126 UT at the harmonic and from about 90 to 20 MHz from 2118 to 2126 UT at the fundamental. This possible secondary type II emission has a significantly lower frequency drift rate, suggesting a shock speed of about only 800 km s^{-1} and an earlier origin time and therefore may not be related to the CME2.

3.2. *White-Light Measurements of the CME Dynamics and Coronal Densities*

CME1 was observed off the east limb in the Mk4 coronameter between 18:50:25 and 19:02:15 UT and in the LASCO C2 and C3 coronagraphs between 19:31:50 UT on January 20 and 00:42:05 UT on January 21. As was particularly evident in the C2 and C3 images, this CME had both a dense inner looplike structure and a fainter outer structure. These two structures, which were significantly separated at large distances, gradually converged with decreasing heliocentric distance. The type II radio emissions, which were generated by a shock driven by this CME, were most likely closely related to the faint leading edge of CME1. For this analysis we therefore used the height-time data for the leading edge of CME1. The actual height-time measurements, made of the leading edge of CME1 at the position angle (PA) of 82° for both Mk4 and LASCO, are shown in Figure 3. The Mk4 data points were the average of several independent measurements, and the uncertainties, shown by the error bars on the Mk4 points, were estimated from the accuracy of identifying the leading edge of the CME. The error bars on the LASCO height-time points are estimates of the uncertainty in measuring the same morphological feature from image to image. For this event, the data quality and feature sharpness were considered excellent, and this corresponds to an estimate of about 5% uncertainty in altitude (plane-of-sky distance; St. Cyr et al. 2000).

The solid line in Figure 3 is the weighted (by the height uncertainties) least-squares fit to the height-time data between 1850 and 2218 UT, i.e., before the two CMEs

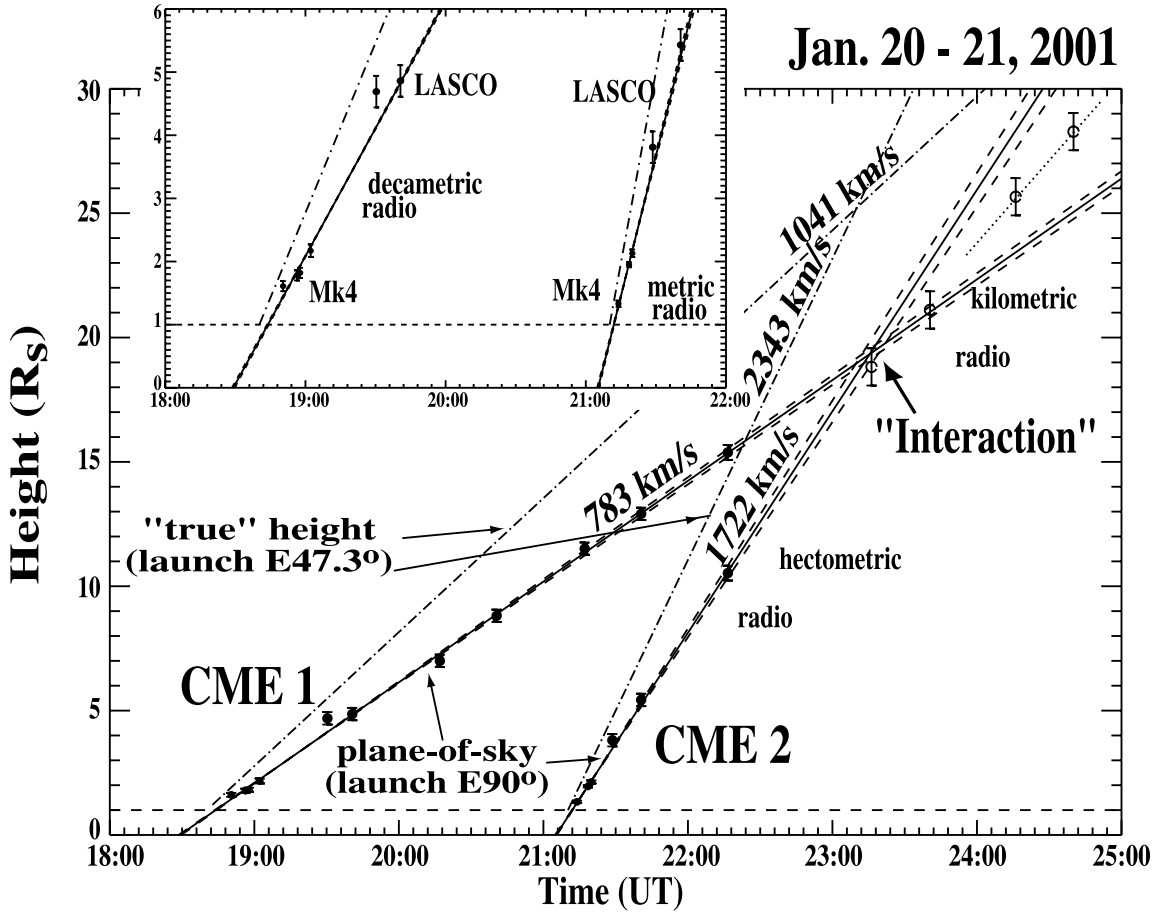

FIG. 3.—Height-time diagram deduced from measurements made from consecutive Mk4 and LASCO images. The solid lines are the weighted fits to the data, as explained in the text, and the dashed lines indicate the range of variation in this fit. The dot-dashed lines are "true" height vs. time plots. (Note that vertical scales for these two sets of lines are slightly different, one corresponding to the plane-of-sky height, the other to the true coronal height.)

merged. This line provides a good fit to both the Mk4 and LASCO data points, except possibly for the first Mk4 point, indicating that the leading edge of CME1 was already moving at a constant speed at 1.8 $R_\odot$ and continued at this constant speed all the way out to $\sim$15 $R_\odot$; i.e., there was no evidence for any significant acceleration. The slope of this weighted straight-line fit gives a plane-of-sky speed of 783.2 ± 10.0 km s^{-1} and a solar liftoff time, projected back to 1 $R_\odot$ (Fig. 3, *horizontal dashed line*), of 18:43.93 $\pm$ 00:00.38 UT. The two dashed lines in Figure 3, derived using the errors in the parameters of the best-fit straight line, indicate the range of fits to the height-time data that are consistent with the measurement uncertainties in each of the data points.

The height-time measurements for CME2, which was first observed in the Mk4 coronameter at 21:13:58 UT, are also displayed on the plot in Figure 3. The leading edge of CME2, which was moving twice as fast as CME1, was observed to apparently overtake and merge with CME1 in the 23:42:31 UT image shown in Figure 1*d*; therefore only the height-time points up to 22:18:05 UT were used to obtain the weighted least-squares fit for CME2. Again, the best-fit straight line (Fig. 3, *solid line*) indicates a CME already moving at a constant speed by the time it reached the coronal height of 1.3 $R_\odot$. The slope of the weighted straight-line fit to these data yields a CME speed of 1721.9 ± 49.2 km s^{-1} and a solar liftoff time, projected to 1 $R_\odot$, of 21:11.99 $\pm$ 00:00.18 UT. As before, the dashed lines show the range of variation in the fit, which is consistent with the measurement uncertainties.

The intersection point of the two straight-line fits indicates that the leading edges of these two CMEs coincided at $\sim$2316 UT. Several height-time points measured after the interaction of these two CMEs are also shown in Figure 3 (*open circles*). If we assume that the combined structure attained a constant speed after the interaction, then from a straight-line fit to the last two height-time points, which occurred well after the interaction, we deduce a speed of $\sim$1266 km s^{-1} for the merged CMEs after the interaction. It is interesting that this final speed is what one would expect for an inelastic collision between the two CMEs, assuming that they have the same mass. No shock or ejecta material was observed at Earth for either of these CMEs.

To compare the radio data in Figure 2 with the dynamics as indicated in Figure 3, we need to know the coronal electron density profile at the time of these two CME events. Fortunately, in addition to measuring the plane-of-sky CME dynamics, the LASCO polarization brightness measurements can also be used to deduce the coronal electron density at different heliocentric distances. These polarized brightness measurements are made at about 2100 UT on each day. Since we wanted to know the electron density profile of the "quiet" corona prior to these CME events, we determined the coronal densities from the white-light polarized measurements at about 2100 UT on 2001 January 19 (there was no significant CME or other coronal activity observed between this time and the liftoff of CME1, which could have disturbed the corona). The electron densities measured in the field of view of the C2 coronagraph are shown by the dashed curve in Figure 4*a*. These volume densities were measured at PA = 72°, close to the points where the white-light measurements were made.

These LASCO density measurements, of course, can be made only for heliocentric distances greater than 2 $R_\odot$, which correspond to radio frequencies below 14 MHz, i.e., for radio emissions observed in RAD2. To interpret the metric radio data, we need to know the coronal densities much closer to the Sun, i.e., outside the spatial range of the LASCO measurements. Therefore we will, in the analyses below, use the Saito (1970) model. The solid curve in Figure 4*a* shows the density profile that corresponds to the Saito (1970) white-light K corona model. The Saito (1970) model was derived from data from 1 to $\geq$4 $R_\odot$ and is expected to be valid at least out to 5 $R_\odot$. As can be seen, the LASCO measurements from 2 to 7 $R_\odot$ agree very well with the Saito (1970) model density profile (which in fact was measured at solar minimum); the measured LASCO densities have essentially the same radial dependence and were about 10% higher than those of the Saito (1970) model. The agreement of the radial dependence of the Saito (1970) model density with that derived from LASCO, in the region where they overlap, to some extent justifies using the Saito model densities for radii less than 2 $R_\odot$ for these CME events.

We also measured the LASCO coronal densities at the same PA at $\sim$2100 UT on January 20, after CME1 passed through the corona. This density profile is shown by the dot-dashed curve in Figure 4*a*. It represents about a 60% increase in electron density.

Finally, we show in Figure 4*b* a contour plot of the electron densities measured by LASCO from PA = 0° to 180° (eastern solar limb) on January 19. On this plot several high-density streamers are evident, e.g., near PA = 20°, 60°, and 100°.

3.3. *Constraints on CME Dynamics from Combined Radio and White-Light Measurements*

In the preceding sections we presented the radio and white-light observations separately. In this section, we demonstrate how the combined radio and white-light data can be utilized to constrain the range of possible CME dynamics. In particular, we will try to estimate the true CME dynamics by requiring consistency between the observed frequency drift rates for the type II radio emissions and the white-light height-time measurements. In making these comparisons between the radio and white-light observations, we are tacitly assuming that the dynamics implied by the radio emissions (from the CME shock) is closely related to the dynamics implied by the leading edge of the CME. We also assume that the longitude of the centroid of the radio sources is close to the solar longitude of the erupting CME. If these assumptions are invalid, then we expect to find inconsistencies in the interpretations of the radio and white-light data, as will be clear below.

To directly compare the white-light coronagraph data with the radio data, we must convert the height-time data, shown in Figure 3, to a frequency versus time curve that corresponds to the CME dynamics. This can be done only after we know (or assume) the coronal density profile, since the density profile allows us to convert each height measurement to a value of the coronal density. The corresponding frequencies, f, are then simply obtained from the square root of the coronal density ($f = f_p = 9\sqrt{n_p}$, fundamental, and $f = 2f_p$, harmonic, where f is in kilohertz and n_p is cm^{-3}).

We have in this way converted the height-time straight line for CME1, using the derived LASCO density profile, to a frequency versus time curve, which we have then overlaid

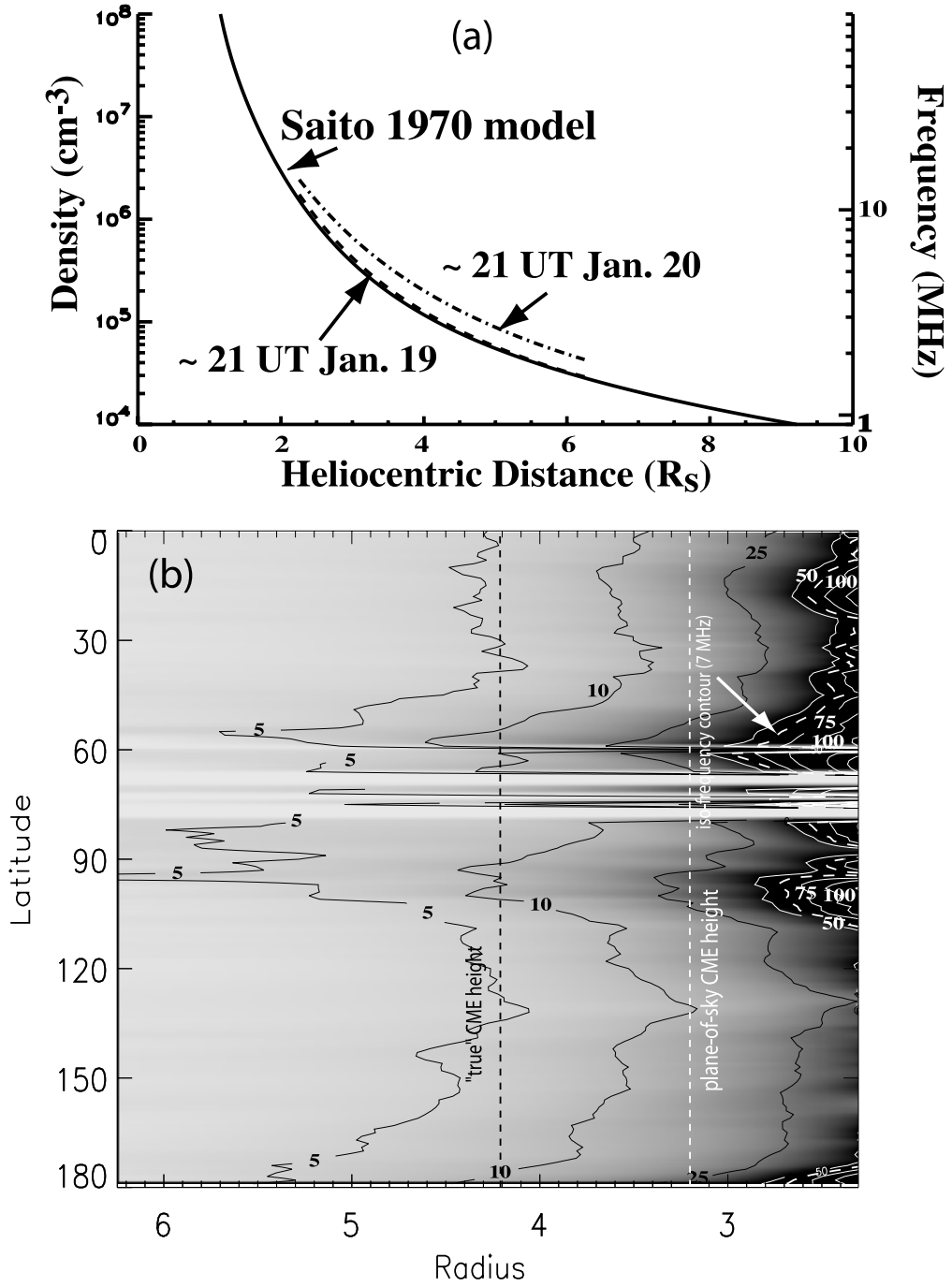

FIG. 4.—(*a*) Coronal densities measured as a function of heliocentric distance from the C2 coronagraph on LASCO by using the polarized brightness measurements. The solid line is the Saito (1970) coronal density profile. (*b*) Contour plot of the corona densities measured by LASCO. The units labeled on the contours are cm^{-3} per 10,000. The white dashed line is the isodensity contour that corresponds to a radio frequency of 7 MHz. Streamer structures at various PAs are evident.

on the radio dynamic spectrum in Figure 2*b* (*yellow dot-dashed curves*). We get two such curves because the radio emissions can be generated at the fundamental (F) and/or harmonic (H) of the plasma frequency. Now it has been suggested from a number of observations (Reiner et al. 1998; Thejappa, Bale, & Vinas 1997; Bale et al. 1999) that the type II radiation is generated in the upstream region of the CME-driven shock. Thus, if the type II radio emissions for CME1 were generated in the "quiet" coronal regions upstream from this CME-driven shock, then we would expect the type II radio emissions to lie along one or both of these yellow dot-dashed curves in Figure 2*b*. As can clearly be seen, however, the observed type II radiation generated by CME1 does not lie along either of these two curves. The observed fundamental and harmonic type II radiation is at significantly higher frequencies, suggesting that the radio emissions must have been generated in an enhanced density region of the corona. To determine how much of a density enhancement is required to explain the observed type II radio data, we simply multiplied the Saito (1970) coronal density profile by a constant scale factor, which was then adjusted until the resulting frequency versus time curve did

fit the observed radio-frequency drift. We found that we had to multiply the Saito (1970) model density by a constant scale factor of 1.7 in order that the corresponding frequency versus time curves passed through the observed fundamental and harmonic type II radio emissions. This fit is shown by the white dashed curves in Figure 2*b*. These curves are frequency-time tracks that correspond to a disturbance propagating through the enhanced Saito model corona at a speed of 783 km s^{-1}.

We next turn our attention to a similar analysis of the radio and white-light data for CME2. Once again we show in the yellow dot-dashed curve in Figure 2*c* the frequency versus time curve expected for fundamental radio emissions by using the measured LASCO coronal density profile. For comparison we also show for this event (*yellow dotted curve*) the frequency versus time curve obtained using the enhanced coronal density profile measured by LASCO at ~21 UT on 2001 January 20 (see Fig. 4*a*). Once again we see that the observed type II emissions occur at consistently higher frequencies than implied by either of these frequency-time curves obtained from the measured LASCO densities at PA = 72°, suggesting that the type II emissions generated by the shock driven by CME2 were also produced in enhanced density regions of the solar corona. As before, we determined the enhancement scale factor required in order that the straight-line fit to the height-time data should fit the observed frequency drift of the type II emissions. The required density enhancement factor for the Saito (1970) model was found to be 3.7, and the resulting frequency versus time curves are shown in the white dashed curves in Figure 2*c*. They correspond to a disturbance propagating through the enhanced Saito model corona at a speed of 1722 km s^{-1}.

As mentioned in § 3.1, for this second CME event there was a clearly defined metric type II radio burst observed semicontinuously over a very wide frequency range, shown in the Culgoora dynamic spectrum included in Figure 2*c*. It is of interest to determine whether the frequency versus time curves that fit the decametric to hectometric type II emissions in Figure 2*c* also fit the frequency drift of this metric type II burst. To check this, by using the Saito (1970) density model we have extrapolated the white dashed curves in Figure 2*c* into the frequency range of the Culgoora observations. Clearly this high-frequency extrapolation does not simultaneously fit the frequency drift of the clearly defined metric type II burst observed by the Culgoora radiospectrograph. Although these curves pass through the region of the more ambiguous metric radio emissions, their frequency drift is too steep to fit any of these slower frequency-drifting emissions, corresponding to possible secondary type II bursts. One possible interpretation of this result is that the metric type II emissions are not dynamically related to decametric type II emissions; i.e., they may have been generated from a different coronal shock (Reiner et al. 2000a). However, for this event there is another possible interpretation because, as we will see, this frequency extrapolation depends on the assumed launch angle and propagation direction of the CME.

In the above analysis we assumed the plane-of-sky dynamics for CME2, which is equivalent to assuming a CME launch and radial propagation from E90°. However, if, for example, we suppose that CME2 and its associated radio sources were launched and propagated radially from a different solar longitude and if we make the simplest geometric corrections for the plane-of-sky projection (namely, "true" height = plane-of-sky height/cosine of the solar longitude), then we will get a different "true" CME height-time relationship for each value chosen for the solar longitude. Then by converting these various height-time lines to the corresponding frequency versus time curves by using the Saito (1970) model, we obtain different extrapolations of the frequency versus time curves to the metric frequencies in Figure 2*c*. In particular, we adjusted the value of the solar longitude until we achieved a "best" fit (determined by eye) to both the decametric and metric type II frequency drift. The solar longitude angle that gave this "best" simultaneous fit was E47°.3 (from Earth). The corresponding height-time relationship is shown by the dot-dashed line for CME2 in Figure 3. The slope of this line yields a "true" or radial CME speed of 2342.6 km s^{-1} and a projected 1 $R_\odot$ time of 2110.2 UT. When we then convert this height-time line to a frequency versus time curve by using the Saito (1970) model, we find that in this case we need to multiply the Saito (1970) model density profile by a scale factor of 8.2 in order that the resulting frequency versus time curves fit the observed decameter to hectometer radio data. The frequency versus time curves corresponding to this fit are shown by the red dashed curves in Figure 2*c*. These curves correspond to the CME/shock propagating through the enhanced Saito model corona with a speed of 2343 km s^{-1}. Clearly, from the fit to the decametric to hectometric radio data alone (*white and red dashed curves*), we cannot distinguish between these two possible dynamical solutions; they give identical fits to these data. However, when these two dynamical solutions for CME2 are then extrapolated to the metric-wavelength range, these frequency versus time curves deviate significantly from each other. In particular, the red dashed curves, corresponding to the CME and radio sources propagating radially from the solar longitude of E47°.3, now precisely fit the frequency drift of the fundamental and harmonic components of the metric type II burst observed by the Culgoora radiospectrograph. This result strongly suggests, first, that the metric type II burst and the decametric to hectometric type II emissions are dynamically related; i.e., both were generated by the same coronal shock. Second, given that both metric and decametric to hectometric type II bursts were generated in this case by the shock driven by CME2, these results then clearly favor the dynamical solution that corresponds to the centroid of the CME and associated radio sources both propagating from a solar longitude of ~E50°.

We can make our arguments more quantitative by determining the (fictitious) solar liftoff times by projecting the fits to both the radio-frequency drift and the fit to the height-time curves back to 1 $R_\odot$ and comparing these two times. First, the best fit to the frequency drift of the metric to hectometric type II radio emissions shown in Figure 2*c* implies a "liftoff" time from 1 $R_\odot$ (corresponding to infinite frequency) of 21:10.2 ± 00:00.1 UT (the time of the metric type II burst is known to an accuracy of at least 6 s). On the other hand, as illustrated in Figure 3, the weighted fit to the CME dynamics, assuming a launch angle of E90°, yields a liftoff time of 21:11.99 ± 00:00.18 UT, whereas the weighted fit corresponding to CME2, propagating radially from the solar longitude of E47°.3, yields a liftoff time of 21:10.2 ± 00:00.12 UT. These results argue compellingly that the latter CME dynamics is consistent with the 1 $R_\odot$ time derived from the frequency drift of the radio data. In

fact, using the statistical errors in the CME liftoff time and speed derived from the fit to the LASCO data in Figure 3 and indicated in the dashed lines in Figure 3, we can estimate the corresponding statistical error in the required CME propagation direction. This was done simply by determining the launch angles required in order that the two dashed lines in Figure 3 should yield frequency-time curves that provide an equally good fit to the frequency-drifting type II emissions shown in Figure 2 (with a slight modification in the scale factor for the density model). We found that the required change in launch angle was $\pm 2\overset{\circ}{.}9$. We therefore conclude that the centroid of the finite CME and its associated radio sources propagated radially from the solar longitude E($47\overset{\circ}{.}3 \pm 2\overset{\circ}{.}9$). This is of course very reassuring since in this case the active region and flare site associated with this CME event was known to be near E46° (§ 3 above).

The above analysis shows how the radio and white-light observations can be combined to constrain the possible dynamics of a CME. One reason that this worked so well in this case was that, on the one hand, the frequency drift of the metric type II burst was very precisely known (to within 6 s) and it was also observed over a very wide frequency range, for which the frequency drift was very steep. On the other hand, the very accurate Mk4 height-time points, which are very near 1 $R_{\odot}$, put a very tight constraint on the projected liftoff time of the CME.

We now return to the results for CME1, which occurred 2.5 hr earlier. In this time the Sun rotated $\sim 1\overset{\circ}{.}5$. Therefore, if we simply assume that CME1 was launched from the exact same solar site, which was then at E$48\overset{\circ}{.}8$, we find the "true" CME height-time relationship shown by the dot-dashed line in Figure 3, whose slope gives a speed of 1040.7 km s^{-1} and a projected 1 $R_{\odot}$ time of 1840.3 UT. Assuming these CME dynamics, we find that we can fit the type II frequency-drifting emissions generated by CME1 if we multiply the Saito (1970) coronal model density by a factor of 5.2. This fit is shown by the red dashed curves in Figure 2*b*.

As can be readily seen, the white and red dashed curves in Figure 2*b* differ significantly from each other, indicating that, at least in principle, from the observed frequency drift of the type II radiation we should be able to easily distinguish between these two solutions, which correspond to very different CME dynamics. However, since for this particular CME event the corresponding type II emissions were observed for only a very brief time interval, it was in fact impossible, in this case, to distinguish between these two different dynamical solutions from these data alone; they are both consistent with the observed radio data. Furthermore, for this event there was no metric type II emission observed by Culgoora that could have further constrained the fit (Culgoora begins its daily operation at ~2000 UT).

3.4. *Source Region of the Type II Radio Emissions*

A major conclusion of the above comparisons between the radio and white-light observations is that the radio emissions must originate from enhanced density regions in the corona. This result is very reminiscent of comparisons that were made between the metric type II bursts and white-light CMEs in the 1980s. For example, a number of investigators found that, in order that the height-time plots derived from the metric type II frequency drift be consistent with the white-light height-time data extrapolated to the same spatial region as the metric type II burst, it was necessary to multiply the coronal density models by factors varying between 3 and 10 (Stewart et al. 1982; Robinson & Stewart 1985). Of course, such comparisons tacitly assumed that the metric type II burst and the white-light data were dynamically related; i.e., the radio emissions were generated by the CME. Unfortunately, decametric to hectometric radio observations were unavailable at that time. Nevertheless, although these earlier results suggested that the type II emissions were generated in enhanced density regions, it was impossible to identify those coronal enhanced density regions from the available data.

With the decametric to hectometric radio data currently available from the unique radio receivers on the *Wind* spacecraft, we have the advantage of observing radio emissions that were generated in the same spatial regions as the corresponding observed white-light CMEs. Thus no spatial extrapolation is involved in comparing the dynamics implied by the white-light CME images with the dynamics implied by the frequency-drifting type II radio emissions. It is significant then from the above analyses of the type II radio emissions in the decametric to hectometric regime, where we are quite confident that the type II radio emissions are generated by the CME/shock, that we have also come to the conclusion, at least for this event, that the radio emissions must have originated in enhanced density regions, with enhancement factors on the order of 5.2 to 8.2 times the Saito (1970) model. It is interesting and perhaps significant that the increase in density implied by the multiplicative factors required to fit the Saito (1970) model for these two CME events is essentially the same as the increase in the LASCO-deduced densities (~60%) observed between these two CME events (Fig. 4*a*).

Furthermore, from the LASCO coronagraph measurements we can derive the coronal densities in the same spatial regions of the corona where these type II radio emissions must originate. Then since the observed radio frequency precisely measures the plasma density in the radio source region, we therefore expect, in principle, to be able to directly identify specific density structures in the corona that may correspond to the locations of the type II radio sources.

Generally speaking, there are two obvious coronal structures that have enhanced densities, the CME itself and coronal streamers. In the 1980s, to explain the fact that the type II emissions originated in regions of enhanced density, Wagner & MacQueen (1983) proposed that the metric type II radio bursts were produced when coronal blast wave shocks propagated through high-density plasma in the legs of a CME that previously lifted off from the Sun. (This scenario also suggested that the metric type II bursts were not produced by CME-driven shocks.)

Since CME1 was propagating through a "quiet" corona and CME2 was propagating through a corona disturbed by the ejection of CME1, with the Wagner & MacQueen (1983) scenario in mind it might therefore be expected that the density enhancement factor required to explain the radio emissions associated with CME2 would have been significantly higher than for those associated with CME1, which propagated through the "quiet" corona. It was rather surprising then that the density enhancement factor for the CME1 and CME2 events turned out to be similar (factor of 5.2–8.2 times the Saito 1970 model). This result seems to suggest that the radio emissions generated by CME2 probably did not originate in high-density legs of CME1, in which case we might have expected enhancement factors of, say, 5–10.

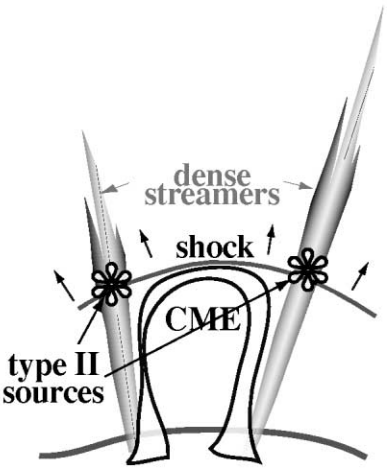

FIG. 5.—Cartoon illustrating the possible scenario for the generation sites of the type II radio emissions associated with these two CME events.

Rather, the type II emissions for these two CME events of 2001 January 20 seem to have been generated in an enhanced density region of the corona, which did not change significantly between the ejection of CME1 and CME2.

On the basis of these observations, we speculate that the metric to hectometric type II radio emissions for the January 20 CME events were generated as the shock, driven by the CME, propagated through high-density coronal streamers as shown schematically in Figure 5. Since the coronal streamers are often not significantly affected by the ejection of a CME (Subramanian et al. 1999), this may provide a simple explanation of why the density enhancement factor required to simultaneously fit the radio and white-light data was similar for both CME events. Such a picture is not inconsistent with interplanetary observations of type II radio emissions. Since we do not have radio imaging, we do not know precisely where along the shock front the type II emissions originate. For interplanetary observations, for which the direction of the radio source can be measured, it is found that the type II radio sources generally appear at different locations along the shock front at different times. Furthermore, the interplanetary observations indicate the shock can extend well beyond the dimensions of the driver CME, since CME-associated shocks are often observed at 1 AU without any evidence of the driver CME. Furthermore, the interplanetary observations suggest that the CME-driven shocks are approximately spherical near the centroid of propagation of the CME. On the other hand, although the radio emissions could also originate near the far flanks of the shock and therefore closer to the Sun where the density would be higher, if this were the case here it would not be possible to match the speed profile implied by the frequency drift with that deduced from the white-light speed profile, since the propagation speed of the flank of a shock is usually significantly lower than the speed along the centroid of the CME (Reiner & Kaiser 1999b).

From an examination of the LASCO movies it appears that one possible candidate is the streamer at PA = 60°. This streamer was still well defined on the 1854 UT January 20 image. In the next image, at 1931 UT, the leading edge of CME1 pushed this streamer to the side (slightly northward), suggesting that it may indeed have been near the CME. After the passage of CME1, this streamer seemed to have been permanently displaced to PA = 52°. (The streamer at PA = 100° also seemed to be pushed to the side by this CME and could also be involved in the type II emissions. Since currently we do not have radio imaging we cannot distinguish between these two possibilities.)

To test this hypothesis, we examined in Figure 4*b* the calculated coronal densities from 2 to 6 $R_\odot$ for all PAs that show clear coronal streamers on the eastern limb at PA = 20°, 60°, and 100°. On this contour plot we have also indicated the isodensity contour (*white dashed contour*) that corresponds to the (fundamental) radio frequency of 7 MHz, observed for CME1 at ~1915 UT. This frequency corresponds to a coronal density of 605,000 cm^{-3}. Clearly, the type II radio emissions observed at 7 MHz must originate from somewhere along this isodensity (or equivalently, isofrequency) contour. As can be seen, the maximum radial extent of this isofrequency contour is 3 $R_\odot$, corresponding to the dense coronal streamer at about PA = 60°. However, at the time (~1915 UT) of this 7 MHz radiation, as can be seen from the CME height-time plot in Figure 3, the leading edge of CME1 was already at a plane-of-sky distance of ~3.2 $R_\odot$, corresponding to an estimated "true" height of ~4.2 $R_\odot$ (Fig. 4*b*, *dashed lines*). Now the highest density along this black dashed line is only ~150,000 cm^{-3}, a factor of 4 too low to explain the observed radio emissions at 7 MHz. Thus even the enhanced densities in the coronal streamers computed by LASCO are apparently not sufficient to account for the observed type II radio emissions at such high frequencies.

However, there is a difficulty with the polarized brightness–derived coronal density measurements because the coronagraphs provide no information on how the density is distributed along the line of sight. Thus we are faced with two options. One is to assume a uniform distribution, and the other is to assume a fixed depth for an enhanced structure (i.e., a streamer). For the LASCO data, as is the usual practice, we assumed an axisymmetric corona. In this case, the observed intensity is assumed to be coming from structures all along the line of sight. During the maximum phase of the solar cycle, a streamer is a confined structure and can be anywhere along the line of sight. Therefore, the polarized brightness inversion techniques generally underestimate the density in the streamers. We tried to estimate the effect of the assumption of an axisymmetric corona on the derived LASCO densities in the following way. We assumed that structures within 80° of the plane of the sky contribute to the observed intensity. Then we calculated the projected (along the line of sight) length of a streamer for different streamer widths as a function of its distance (measured from the streamer central axis) from the plane of the sky. Then we took the ratio of the projected streamer length over the "total" length between ±80°. These calculations refer to a projected height of 3 $R_\odot$ and assume that the streamer is the only structure along the line of sight. These ratios are then estimates of the correction factor of the LASCO densities for a confined streamer. Figure 6 shows a plot of the correction factor as a function of the angular distance of the streamer from the plane of the sky for several different streamer widths. As can be seen from the plot, one can easily obtain density enhancement factors of ~4, at an angular distance of 40° from the plane of the sky, for a streamer of width 40°–50°. This would then be sufficient to bring the density of the coronal streamer, say at PA = 60°, into agreement with the density implied by the observed radio

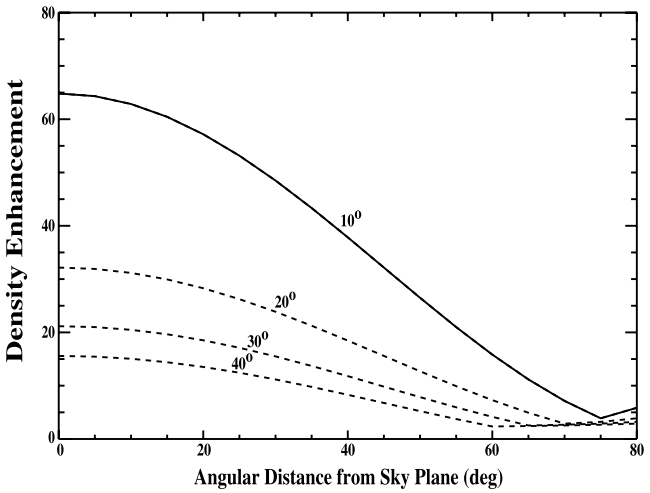

FIG. 6.—Plot showing the density enhancement as a function of angular distance from the plane of the sky for four different streamer widths.

emission for CME1. In fact, we can use these results to argue that the streamer width implied by the radio and white-light data is of the order of 40° or more. Finally, we should mention that our density enhancement estimates are in general agreement with a more careful study by Leblanc, Leroy, & Poulain (1970). They found factors of 2–4 above the background density for enhancements at the bases of coronal streamers.

4. DISCUSSION

In this paper, we have illustrated how, by requiring consistency between the radio and white-light observations, we can constrain the range of possible CME dynamic solutions. For example, we were able to demonstrate that the consistency between the radio and white-light data for the 2001 January 20 CME events suggested a CME/radio dynamics that corresponded to radial propagation from a solar longitude of E($47\overset{\circ}{.}3 \pm 2\overset{\circ}{.}9$). This method works in principle because the radio observations inherently measure the true (radial) dynamics, whereas the white-light observations measure the plane-of-sky dynamics. In making these consistency arguments of course we have also tacitly assumed that the speed of the leading edge of the CME (coronagraph observations) was essentially the same as the speed of the CME-driven shock (radio observations). The overall consistency of the dynamics implied by the radio and white-light observations with the known flare site seems to suggest the validity of this assumption.

All the uncertainties in the physical quantities derived above are statistical errors that result from the least-squares analysis. Of course, in addition there are many systematic errors involved in these measurements that may significantly increase these error estimates. However, the point that we wish to emphasize here about these derived statistical uncertainties is that they dramatically illustrate the intrinsic accuracy of this technique of combining radio and white-light data for estimating the CME dynamics.

The systematic errors, which are difficult to accurately estimate, imply that the actual uncertainties in the derived physical quantities (CME propagation direction, CME speeds, etc.) are larger than those quoted above. These systematic errors include the fact that the radial dependence of the coronal density at low solar altitudes may differ somewhat from that given by the Saito (1970) model, the fact that we have used a very simple plane-of-sky projection correction that does not take into account the finite shape and size of the CME, the fact that the radio sources may not be exactly located near the centroid (" nose ") of the CME, etc. Given these systematic uncertainties, it is probably not unreasonable to expect that our error estimates could be multiplied by a factor of 2 or more, which may increase the uncertainty in the launch angle from $\pm 3^\circ$ to $\pm 6^\circ$ to 10°.

As illustrated in Figures 2*b* and 2*c*, different CME dynamics yields different frequency versus time curves that imply different frequency drift rates for the type II emissions. If the type II radio emissions are observed for a sufficiently long time interval, the different dynamical solutions can be easily distinguished. From the results shown in Figure 2, it is clear that for a relatively slowly moving CME (like CME1) a long period of type II emissions at decametric to hectometric wavelengths should be sufficient to constrain the possible CME dynamics. On the other hand, for fast-moving CMEs, such as CME2 in Figure 2*c*, one may often need the additional metric type II frequency drift rate to sufficiently constrain the CME dynamics.

It is known that the low-frequency kilometric-wavelength type II radio emissions are generated by CME-driven shocks (Cane, Sheeley, & Howard 1987; Bale et al. 1999). Since these kilometric type II radio emissions are often clear continuations of the decametric to hectometric type II emissions, it follows that these decametric to hectometric type II radio emissions are also generated by CME-driven shocks (Reiner & Kaiser 1999b; Reiner et al. 2000a). However, the origin of the metric type II burst is still unclear and controversial (Reiner & Kaiser 1999b; Reiner et al. 2000a; Cliver et al. 1999). One implication of the above analysis is that the metric type II burst observed for the January 20 CME2 event was most likely generated by the associated CME-driven shock. Then since the highest frequency of the metric type II burst (160 MHz) corresponds to a heliocentric distance of $\sim 1.3\ R_\odot$, this suggests that a CME-driven shock (that produces type II emissions) can sometimes form very low in the corona (Dulk, Leblanc, & Bougeret 1999).

Since, using the above methodologies, we have derived rather accurate estimates of the liftoff times of the CMEs, it is of interest to examine the relationship of these times with the times of the solar flares associated with each of these events. In both cases we found that there was no obvious relationship between the derived CME liftoff times and the times associated with the flares. We found that the projected CME liftoff times were ~ 10 minutes earlier than the flare maximum times and at least a few minutes later than the onset time of the flares, suggesting that the associated flares were already in progress when these CMEs lifted off from the Sun.

Our final remarks concern the interactions between these two CMEs. Several height-time points were also measured after CME2 merged with CME1. The last two height-time points in Figure 3 were separately fitted with a straight line. The slope of this line gave a final CME speed of 1266 km s^{-1} (see § 3.2), indicating that after the interaction with CME1, CME2 slowed down by $\sim 25\%$. (Of course, in fitting these latter data to a straight line, it was tacitly assumed that the deceleration associated with this interaction must have occurred over a relatively short time around the interaction

time at 2311 UT.) Thus if the true speed of CME2 was 2343 km s^{-1}, as indicated if the launch angle was $\sim$E50°, then the speed after the interaction was probably reduced to $\sim$1724 km s^{-1}, as would be expected for an inelastic collision between two approximately equal-mass CMEs. Furthermore, it has been argued (Gopalswamy et al. 2001; Reiner et al. 2001) that CME interactions are often accompanied by a sudden increase in the bandwidth and intensity of the radio emissions. Although it is not so clear from the dynamic spectrum shown in Figure 2, a careful examination of the individual intensity profiles at each observing frequency suggests that between about 2200 and 2220 UT the type II emissions were observed from 1.6 to 3.6 MHz, suggesting a frequency bandwidth, $\Delta f/f$, of about 0.8. However, from 2245 to 2300 UT the type II emissions were observed from 450 kHz to 1.6 MHz, suggesting a frequency bandwidth of 1.2. Furthermore, the maximum intensity of the type II emissions increased from about 32,000 sfu (1 sfu = 10^{-22} W m^{-2} Hz^{-1}) to about 100,000 sfu; about a threefold increase.

If we therefore speculate that the increased radio bandwidth and intensity observed at $\sim$2248 UT was the time of the first contact between CME2 and CME1, then, using the estimated "true" CME speeds, we can estimate the radial thickness of the ejecta associated with CME1 in the upper corona. From the time of first contact to the actual interaction of the two shocks at 2311 UT, CME2 moved a radial distance of $\sim$4.6 $R_\odot = 0.02$ AU, suggesting that this is the approximate diameter of the ejecta material associated with CME1 in the high corona. This is in contrast to the typical diameter of $\sim$65 $R_\odot = 0.3$ AU for a magnetic cloud observed at 1 AU (Burlaga, Lepping, & Jones 1990).

5. CONCLUSION

The method outlined in this paper offers a promising new technique for constraining the dynamics of CMEs by requiring consistency between the simultaneous radio and white-light observations. To our knowledge this is the first time that simultaneous radio and white-light observations have been used to quantitatively constrain the CME dynamics and to deduce the CME propagation direction and corresponding solar launch angle. We have illustrated the technique for two CME events on 2001 January 20, and our analysis indicates that the required consistency between the radio and white-light observations were consistent with a CME propagation direction of E($47^\circ.3 \pm 2^\circ.9$), which agrees very well with the known flare site. We also showed that consistency between radio and white-light data implied that the radio emissions must have originated in high-density structures in the corona, and we argued that the data are consistent with an origin of the type II radio emissions in the dense streamers observed at that time in the corona. We have also used these observations to obtain information about the dynamics of the interaction of these two CMEs, suggesting a 25% decrease in the speed of the fast CME after the interaction and a radial dimension of the CME ejecta in the high corona of $\sim$5 $R_\odot$.

It is anticipated that techniques such as those used here will be used to even greater advantage for the radio and coronagraph observations in the upcoming STEREO mission.

The *Wind* WAVES experiment is a collaboration of NASA/Goddard Space Flight Center, the Observatoire de Paris-Meudon, and the University of Minnesota. *SOHO* is an international collaboration between NASA and ESA. LASCO was constructed by a consortium of institutions: the Naval Research Laboratory (Washington, DC), the Max-Planck-Institut fur Aeronomie (Katlenburg-Lindau, Germany), the Laboratoire d'Astronomie Spatiale (Marseille, France), and the University of Birmingham (Birmingham, UK). M. J. R. acknowledges support in part from NSF grant ATM 01-12186. O. C. S. acknowledges partial support from NSF grant ATM 98-19668 and NASA contract S-86760-E. A. V. acknowledges support from NASA contracts, and R. A. H. acknowledges support from NASA contracts and the Office of Naval Research.

REFERENCES

Bale, S. D., Reiner, M. J., Bougeret, J.-L., Kaiser, M. L., Krucker, S., Larson, D. E., & Lin, R. P. 1999, Geophys. Res. Lett., 26, 1573
Bougeret, J. L., et al. 1995, Space Sci. Rev., 71, 231
Brueckner, G. E., et al. 1995, Sol. Phys., 162, 357
Burlaga, L. F., Lepping, R. P., & Jones, J. A. 1990, in Geophysical Monograph Ser. 58, Physics of Magnetic Flux Ropes, ed. T. Russell et al. (Washington: AGU), 373
Cane, H. V., Sheeley, N. R., Jr., & Howard, R. A. 1987, J. Geophys. Res., 92, 9869
Cliver, E. W., Webb, D. F., & Howard, R. A. 1999, Sol. Phys., 187, 89
Dulk, G. A., Leblanc, Y., & Bougeret, J.-L. 1999, Geophys. Res. Lett., 26, 2331
Elmore, D. F., Burkepile, J. T., Darnell, J. A., Lecinski, A. R., & Stanger, A. L. 2003, Proc. SPIE, vol. 4823
Eselevich, V. G., & Filippov, M. A. 1991, Planet. Space Sci., 39, 737
Fainberg, J., & Stone, R. G. 1971, Sol. Phys., 17, 392
Fisher, R. R., & Munro, R. H. 1984, ApJ, 280, 428
Gopalswamy, N., Kaiser, M. L., Kahler, S. W., Ogilive, K., Berdichevsky, D., Kondo, T., Isobe, T., & Akioka, M. 1998, J. Geophys. Res., 103, 307
Gopalswamy, N., Yashiro, S., Kaiser, M. L., Howard, R. A., & Bougeret, J.-L. 2001, ApJ, 548, L91
Gopalswamy, N., et al. 2000, Geophys. Res. Lett., 27, 1427
Hayes, A. P., Vourlidas, A., & Howard, R. A. 2001, ApJ, 548, 1081
Howard, R. A., Michels, D. J., Sheeley, N. R., Jr., & Koomen, M. J. 1982, ApJ, 263, L101
Hundhausen, A. J., Burkepile, J. T., & St. Cyr, O. C. 1994, J. Geophys. Res., 99, 6543
Jones, D., et al. 2000, in Geophysical Monograph Ser. 119, Radio Astronomy at Long Wavelengths, ed. R. G. Stone et al. (Washington: AGU), 339
Kaiser, M. L., Reiner, M. J., Gopalswamy, N., Howard, R. A., St. Cyr, O. C., Thompson, B. J., & Bougeret, J.-L. 1998, Geophys. Res. Lett., 25, 2501
Leblanc, Y., Dulk, G. A., & Bougeret, J.-L. 1998, Sol. Phys., 183, 165
Leblanc, Y., Dulk, G. A., Vourlidas, A., & Bougeret, J.-L. 2001, J. Geophys. Res., 106, 25301
Leblanc, Y., Leroy, J. L., & Poulain, P. 1970, A&A, 5, 391
Newkirk, G., Jr. 1967, ARA&A, 5, 213
Plunkett, S. P., Thompson, B. J., Howard, R. A., Michels, D. J., St. Cyr, O. C., Tappin, S. J., Schwenn, R., & Lamy, P. L. 1998, Geophys. Res. Lett., 25, 2477
Prestage, N. P., Luckhurst, R. G., Paterson, B. R., Bevins, C. S., & Yuile, C. G. 1994, Sol. Phys., 150, 393
Reiner, M. J., & Kaiser, M. L. 1999a, Geophys. Res. Lett., 26, 397
———. 1999b, J. Geophys. Res., 104, 16979
Reiner, M. J., Kaiser, M. L., & Bougeret, J.-L. 2001, J. Geophys. Res., 106, 29989
Reiner, M. J., Kaiser, M. L., Fainberg, J., & Stone, R. G. 1998, J. Geophys. Res., 103, 29651
Reiner, M. J., Kaiser, M. L., Plunkett, S. P., Prestage, N. P., & Manning, R. 2000a, ApJ, 529, L53

Reiner, M. J., Karlický, M., Jiřička, K., Aurass, H., Mann, G., & Kaiser, M. L. 2000b, ApJ, 530, 1049
Robinson, R. D., & Stewart, R. T. 1985, Sol. Phys., 97, 145
Saito, K. 1970, Ann. Tokyo Astron. Obs., Ser. 2, 12, 53
St. Cyr, O. C., et al. 2000, J. Geophys. Res., 105, 18169
Stewart, R. T., Dulk, G. A., Sheridan, K. V., House, L. L., Wagner, W. J., Sawyer, C., & Illing, R. 1982, A&A, 116, 217
Subramanian, P., Dere, K. P., Rich, N. B., & Howard, R. A. 1999, J. Geophys. Res., 104, 22321
Thejappa, G., MacDowall, R. J., & Vinas, A. F. 1997, Proc. 31st ESLAB Symp., Correlated Phenomena at the Sun, in the Heliosphere and in Geospace (ESA SP-415; Noordwijk: ESTEC), 189
Thompson, B. J., Plunkett, S. P., Gurman, J. B., Newmark, J. S., St. Cyr, O. C., & Michels, D. J. 1998, Geophys. Res. Lett., 25, 2465
van de Hulst, H. C. 1950, Bull. Astron. Inst. Netherlands, 11, 135
Wagner, W. J., & MacQueen, R. M. 1983, A&A, 120, 136